Soft Matter

Volume 1 | Number 1 | Jan 2013 | Pages 1–100

Soft Matter

www.rsc.org/softmatter

ROYAL SOCIETY OF CHEMISTRY

Illustrating consistency of different experimental approaches to probe the buried polymer/metal interface using sum frequency generation vibrational spectroscopy

Xiaolin Lu[a], Bolin Li[a], Peizhi Zhu[b], Gi Xue[c], Dawei Li*[c]*

[a] *State Key Laboratory of Bioelectronics, School of Biological Science & Medical Engineering, SoutheastUniversity, Nanjing, 210096,Jiangsu Province, P. R. China*

[b] *College of Chemistry and Chemical Engineering, Yangzhou University, Yangzhou 225009, Jiangsu Province, P. R. China*

[c] *Nanjing University, Nanjing 210093, Jiangsu Province, P. R. China*

Abstract: In this paper, we demonstrate our ability to directly probe the molecular structures of the buried polymer/metal interface using sum frequency generation (SFG) vibrational spectroscopy. Spectroscopic data from different experimental approaches were compared and analyzed to deduce the molecular ordering information at a buried polymer/metal interface, i. e. the poly(n-butyl methylacrylate) (PBMA)/silver (Ag) interface. Solid spectroscopic evidence suggested that we successfully detected the molecular vibrational signals generated from the buried PBMA/Ag interface. It was found that the side butyl methyl groups at the PBMA/Ag interface are polar-ordered and have different orientational ordering from those at the PBMA surface in air. We believe this study will provide a useful experimental and analytical framework for the SFG spectroscopy to probe the buried polymer/metal interfaces in the future.

1. Introduction

Polymer materials are widely used in modern industry and daily life. Understanding the polymer interfacial properties, especially for buried interfaces with metals, is of great importance in many applications such as microelectronics, anti-corrosion coating, colloid stabilization, and automotive paints, etc. The macroscopic material interfacial properties including wettability, friction, adhesion as well as compatibility towards applied substrates, to

a large extent, are controlled by microscopic interfacial structures at the molecular or atomic level. In the last few decades, a variety of surface-sensitive techniques have been developed [1-10]. However, probing a buried polymer interface is still extremely challenging. On account of this, the techniques which can characterize the molecular structures of buried polymer interfaces *in situ* are still in great demand. Recently, Sum Frequency Generation (SFG) vibrational spectroscopy has been developed into a unique technique to investigate surface and interfacial structures of various polymer materials. With inherently interfacial selectivity and submonolayer sensitivity, SFG can directly detect buried solid interfaces without breaking it [11-17]. However, till now only a few studies have been focused on probing the buried polymer/metal interfaces. For example, the molecular structures of the poly(methyl methacrylate) (PMMA)/silver (Ag) interface were investigated for PMMA films spin-coated onto the Ag substrates where the SFG resonant signals from both the PMMA surface in air and PMMA/Ag interface were detected simultaneously [15]. Later on a new experimental methodology to directly probe a buried polymer/metal interface *in situ* was developed where a poly(methyl acrylate) (PMA) polymer film was sandwiched between a transparent fused silica window and a silver substrate. The SFG vibrational signal contributed from the silica/PMA interface was found to be negligible compared to that from the buried PMA/Ag interface. Therefore, the SFG resonant signals were dominated by the contribution from the polymer/metal interface [16]. Recently, it was found that a buried polymer/metal interface can also be directly probed by using a special light polarization-combination (ppp, p-polarized sum frequency signal, p-polarized visible beam, and p-polarized IR beam) in this nonlinear spectroscopic experiment [17]. Here we combine the three methodologies to probe a new buried polymer/metal interface, i.e. the poly(butyl methacrylate) (PBMA)/Ag interface. Both ssp and ppp spectra were collected in the normal face-up and sandwiched geometries. The consistence of the experimental results and data interpretation were confirmed that such methodologies we developed can be generally applied to study the buried polymer/metal interfacial molecular structures.

2. Experimental Section

2.1 SFG vibrational spectroscopy

The infrared-visible SFG system in this study is a custom-designed Ekspla SFG spectrometer (EKSPLA, Lithuania). The fixed 532-nm-wavelength visible beam was generated by frequency-doubling the fundamental output pulses of 20 ps width with a 1064-nm wavelength from a Nd:YAG laser. An optical parametric generation/amplification (OPG/OPA) and difference frequency generation (DFG) system based on LBO and $AgGaS_2$ crystals was used to generate the tunable infrared (IR) beam. The visible and tunable IR beams were overlapped on the sample surface with incidence angles of 60° and 57° respectively and the output angle of the sum frequency signals was ~59°. The diameter of the overlapped beam spot at the sample surface was around 0.5 mm. The input visible and IR beam powers were monitored by collecting parts of the reflections via two photodiodes. The output sum frequency signals were collected via a monochromatic spectrograph in terms of the input IR frequency (wavenumber, cm^{-1}). The SFG signals were then normalized by the input powers of the visible and IR beams. In this particular study, three different experimental geometries for collecting the SFG spectra were used, as shown in Figure 1. In Panel A of Figure 1, a polymer film was deposited on a silica window substrate and the output SFG signal was directly collected from the surface. In Panel B of Figure 1, a polymer thin film was sandwiched between a silica window and an Ag substrate; the input visible and IR beam went through the transparent silica window and overlapped at the polymer/Ag interface; and the output SFG signals also went through the transparent silica window first and then were collected by our monochromator. In Panel C of Figure 1, a polymer thin film was deposited on an Ag substrate; the output signals from both the polymer surface in air and the polymer/Ag interface were collected. For all the three geometries, the vibrational signals in the C-H range from 2800 cm^{-1} to 3050 cm^{-1} were collected.

2.2 Sample preparation

Poly(n-butyl methacrylate) (PBMA) was purchased from Scientific Polymer Products Inc. (M_W=180,000) and used as received. The fused silica windows of 1 in. diamter and 1/8 in. thickness were purchased from Esco Products, Inc. Before sample preparation, the fused silica windows were sequentially treated with a sulphuric acid bath saturated with potassium dichromate, air plasma and piranha solution bath. PBMA films were prepared by spin-coating PBMA solution (in toluene) onto the silica window substrates (Panel A in Figure 1) or Ag

3

substrates (Panel C in Figure 1). The Ag substrates were prepared by depositing a 200-nm thick Ag layer on the silica windows (with a 15-nm thick nickel layer in between to increase the adhesion) via an electron-beam evaporator (Cooke Evaporator, Cooke Vacuum Products). For the sandwiched geometry (Panel B in Figure 1), a 200-nm thick Ag layer was deposited on top of the PBMA thin films which were previously prepared on the silica windows. All the samples were annealed at 80 °C for 1 hour again before the SFG experiment. For the sandwiched geometry, the PMMA films on the silica windows before Ag deposition were pre-annealed at 80 °C for 1 hour.

2.3 Theoretical Background

A sum frequency generation process involves two incoming beams and one output beam, i.e. input visible, input infrared and output sum frequency beams, respectively. As a second-order nonlinear optical spectroscopy, the SFG process is forbidden in centro-symmetric materials but allowed at the surfaces or interfaces where the inversion symmetry is necessarily broken under the electric dipole approximation [18]. Such a selection rule makes the SFG vibrational spectroscopy extremely surface and interface sensitive and renders to it the ability to detect the molecular vibrational signals at the surfaces and interfaces. An SFG spectrum can be obtained by plotting the sum frequency intensity as a function of the input IR frequency. The intensity of the output sum frequency signal in the reflection mode can be written as [19]

$$I(\omega) = \frac{8\pi^3 \omega^2 \sec^2 \beta}{c^3 n_1(\omega_1) n_1(\omega_2) n_1(\omega)} \left| \chi_{eff}^{(2)} \right| I_1(\omega_1) I_2(\omega_2) AT \qquad (1)$$

Where $n_1(\omega_i)$ is the frequency (ω_i) dependent refractive index of the medium. β is the output sum frequency reflection angle. $I_1(\omega_1)$ and $I_2(\omega_2)$ are the intensities of the input visible and IR fields, respectively. T is the input beam pulse-width. A is the overlapping area of the two input beams at the sample surfaces or/and interfaces. $\chi_{eff}^{(2)}$ is the effective second-order nonlinear optical susceptibility. Optically, the input and output beams can be adjusted s- or p-polarized. Therefore, different components of $\chi_{eff}^{(2)}$ can be experimentally measured with different polarization combinations, such as the following ssp (s-polarized sum frequency signal, s-polarized visible beam, and p-polarized IR beam), sps, pss, and ppp polarization combinations [19].

$$\chi_{eff,ssp}^{(2)} = L_{yy}(\omega)L_{yy}(\omega_1)L_{zz}(\omega_2)\sin\beta_2\chi_{yyz} \quad (2\text{-}1)$$

$$\chi_{eff,sps}^{(2)} = L_{yy}(\omega)L_{zz}(\omega_1)L_{yy}(\omega_2)\sin\beta_1\chi_{yzy} \quad (2\text{-}2)$$

$$\chi_{eff,pss}^{(2)} = L_{zz}(\omega)L_{yy}(\omega_1)L_{yy}(\omega_2)\sin\beta\chi_{zyy} \quad (2\text{-}3)$$

$$\begin{aligned}
\chi_{eff,ppp}^{(2)} = &-L_{xx}(\omega)L_{xx}(\omega_1)L_{zz}(\omega_2)\cos\beta\cos\beta_1\sin\beta_2\chi_{xxz} \\
&-L_{xx}(\omega)L_{zz}(\omega_1)L_{xx}(\omega_2)\cos\beta\sin\beta_1\cos\beta_2\chi_{xzx} \\
&+L_{zz}(\omega)L_{xx}(\omega_1)L_{xx}(\omega_2)\sin\beta\cos\beta_1\cos\beta_2\chi_{zxx} \\
&+L_{zz}(\omega)L_{zz}(\omega_1)L_{zz}(\omega_2)\sin\beta\sin\beta_1\sin\beta_2\chi_{zzz}
\end{aligned} \quad (2\text{-}4)$$

Here there are seven tensor components of second-order nonlinear susceptibility (χ_{yyz}, χ_{yzy}, χ_{zyy}, χ_{xxz}, χ_{xzx}, χ_{zxx}, and χ_{zzz}) defined in the lab coordinate system with z axis defined as the surface normal and xz plane containing the input and output beams (see Panel D in Figure 1). β, β_1 and β_2 are the output angle for the sum frequency signal, input angle of the visible beam and input angle of the IR beam. L_{ii}s are (i=x, y, or z) the Fresnel coefficients responsible for the local field correction of the two input and one output beams. For a surface or interface embedded between two semi-infinite media, L_{ii}s can be written as [19-21]

$$L_{xx}(\omega) = \frac{2n_1(\omega)\cos\gamma}{n_1(\omega)\cos\gamma + n_2(\omega)\cos\beta} \quad (3\text{-}1)$$

$$L_{yy}(\omega) = \frac{2n_1(\omega)\cos\beta}{n_1(\omega)\cos\beta + n_2(\omega)\cos\gamma} \quad (3\text{-}2)$$

$$L_{zz}(\omega) = \frac{2n_2(\omega)\cos\beta}{n_1(\omega)\cos\gamma + n_2(\omega)\cos\beta} \cdot \left(\frac{n_1(\omega)}{n'(\omega)}\right)^2 \quad (3\text{-}3)$$

Such equations are valid for both the sum frequency, visible and IR beams. $n'(\omega)$ is the refractive index of the surface or interfacial layer. β is the beam input or output angle and γ is the refracted angle in the medium 2. An infrared-resonant SFG spectrum can be fitted using the following equation when the infrared frequency is near the vibrational resonance.

$$\chi_{ijk}^{(2)} = \chi_{NR} + \sum_q \frac{A_q}{\omega_2 - \omega_q + i\Gamma_q} \quad (4)$$

χ_{NR} is the non-resonant background arising from the electric polarization of the surface or interface and the adjacent media. A_q, ω_q, and Γ_q are the strength, resonant frequency, and damping coefficient of the vibrational mode q, respectively.

At an azimuthally isotropic surface or interface, only four independent nonzero second-order nonlinear susceptiblity tensor components exist, which are [22]

$$\chi_{xxz} = \chi_{yyz}, \chi_{xzx} = \chi_{yzy}, \chi_{zxx} = \chi_{zyy}, \chi_{zzz} \qquad (5)$$

Through transferring from the molecular coordinate to the lab coordinate system, the relationship between the tensor components of the macroscopic second-order nonlinear susceptibility and the tensor components of the molecular hyperpolarizability can be built up, which can be used for orientation calculation (see Supplementary Information for the methyl groups discussed in this paper).

3. Results and Discussion

3.1 SFG spectra of PBMA surface in air

Poly(n-butyl methylacrylate) (PBMA) is a thermoplastic material which has broad applications in engineering coating and composite materials. Its relatively long butyl acrylate groups make it a flexible elastomeric material at room temperature. Previous studies have shown that for thin films of hydrophobic polymers deposited on the silica substrates, the surface contribution dominates the SFG output in the CH frequency range (2800 cm^{-1} to 3050 cm^{-1}), where the vibrational bands of methyl, methylene, and methenyl groups locate [23-25]. Figure 2 shows the ssp and ppp spectra of the PBMA surface in air collected from a 200-nm thick PBMA film on a silica substrate. In ssp spectra, the symmetric stretching (ss) mode at 2880 cm^{-1} and Fermi resonance (Fermi) at 2935 cm^{-1} of the side ester butyl methyl groups are the two strongest modes. In ppp spectra, the anti-symmetric stretching (as) mode of the methylene groups at 2910 cm^{-1} and the as mode of the ester butyl methyl groups at 2960 cm^{-1} are the two strongest modes. It should be noted that the collected ssp spectrum shows the similar spectral characteristics to the previously published one [26], indicating a mutual consistency exists. Table 1 shows the fitting results for the SFG spectra in Figure 1. Based on the strong resonant signals in these spectra and the previous SFG study on the PBMA surface by Wang et. al. [26], we can know that the side ester butyl methyl groups are polar-ordered at the surface tilting towards the air side. From the energy viewpoint, this type of orientational ordering can present the low energy methyl groups at the surface to minimize the surface free

energy. Besides, the side methyl groups connecting to the three methylene groups are highly mobile compared to the backbone segments and the α-methyl groups. With the ester butyl methyl groups pointing to the air side, the mobile side chains can seek the maximum free volume at the air side to maximize the possible conformations. Although it is interesting to see both enthalpy and entropy favor the absolute orientation of the side methyl groups, i.e. pointing to the air side, different conformations or conformational change of the side chains can render the different orientation angles of the methyl groups at the surface. This should be the intrinsic reason why certain distribution, for instance Gaussian distribution, is generally used to describe the orientation angles of the molecular groups for organic materials, especially polymers.

3.2 SFG spectra of PBMA sandwiched between silica and Ag

In this experimental setup, the sample geometry is a PBMA thin film sandwiched between a silica substrate and a thick Ag layer. As shown in Panel B of Figure 1, the input visible and infrared beams penetrated through the transparent silica window and overlapped at the PBMA/Ag interface. The output sum beam reflected back through the silica and then was collected. In this case, there are still two interfaces, namely, the silica/PBMA and PBMA/Ag interfaces, both of which could generate the SFG resonant signals. However, two advantages using this sandwiched geometry must be mentioned. One is the suppressed ordering of the hydrophobic groups at the silica/PBMA interface due to the hydrophilic nature of the silica surface. The other is the nearly constant visible and infrared light fields reaching the PBMA/Ag interface no matter what the PBMA film thickness is due to the similar refractive indexes of silica and PBMA; and a constant SFG resonant output from the PBMA/Ag interface is thus expected [16].

Figure 3 shows the ssp and ppp spectra from the sandwiched geometry with different film thicknesses. The spectra in the right graphs were offset for clarity. Different from the surface PBMA spectra collected from a PBMA thin film on a silica substrate, the interfered spectra were observed for both ssp and ppp polarization combinations because of the effect of the strong non-resonant background generated from the Ag surface. In ssp spectra, the apparent positive peak at around 2860 cm^{-1} comes from the ss mode of the methylene groups and the apparent negative peak at around 2956 cm^{-1} comes from the as mode of the ester butyl methyl

7

groups [26]. In ppp spectra, the apparent two negative peaks at 2875 cm^{-1} and 2935 cm^{-1} are assigned to the symmetric stretching (ss) mode and Fermi resonance of the ester butyl methyl groups, respectively [26].

Table 2 shows the fitting results for the spectra in Figures 3. The independent ssp and ppp spectral features on the film thickness provide the direct experimental evidence that these vibrational resonances were generated from the PBMA/Ag interface. If any significant vibrational resonance came from the silica/PBMA interface, different interfered spectral patterns would be observed because of the signal interference from the silica/PBMA interface when the film thickness changed.

Figure 4 shows the calculated Fresnel coefficients for the silica/PBMA and PBMA/Ag interface. It is pretty clear, whether for ssp or ppp polarization combination, the Fresnel coefficients for the PBMA/Ag interface keep almost constant while the Fresnel coefficients for the silica/PBMA change significantly with varying thickness. This calculation provides further evidence that the ssp and ppp resonant signals for the sandwiched geometry come solely from the PBMA/Ag interface. Therefore, such a sandwiched geometry works pretty well for probing the resonant signals of the PBMA/Ag interface by suppressing the signals generated from the other interface, i.e. the silica/PBMA interface.

3.3 SFG spectra of PBMA films on Ag substrates

Figure 5 shows the ssp and ppp spectra for PBMA films with different thicknesses directly deposited on the Ag substrates (Panel C in Figure 1). The ssp spectra show strong dependence on the film thickness while the ppp spectra show almost no dependence on the film thickness. The PBMA surface in air and the PBMA/Ag interfaces could both contribute to the SFG resonant signals and the relative intensities of the two interfaces should be determined by the Fresnel coefficients responsible for the local field correction. We followed the previous methods [15, 25, 27-31] to calculate the Fresnel coefficients of the PBMA surface in air and the PBMA/Ag interface for ssp polarization combination. The calculated surface Fresnel coefficient $F_{Air-PBMA}$ and interfacial Fresnel coefficient $F_{PBMA-Ag}$ as a function of film thickness were shown in Panel A of Figure 6. It was found that $F_{Air-PBMA}$ is much larger than $F_{PBMA-Ag}$, suggesting the resonant signals from the PBMA surface in air prevailed over those from the PBMA/Ag interface through the discussed thickness range. Indeed, all

the ssp spectra of PBMA films with different thicknesses showed the surface spectral feature (Figure 2), evidenced by the two strong modes of methyl ss mode at 2875 cm^{-1} and methyl Fermi resonance at 2935 cm^{-1}. Furthermore, using the normalized surface and interfacial ssp resonant signals, plus an adjustable non-resonant background and calculated Fresnel coefficients, the ssp SFG spectra of PBMA films on the Ag substrates can be reconstructed. The reconstructed ssp spectra are shown as the solid lines in Panel B of Figure 5. The details on the reconstruction of the spectra can be found in Supplementary Information.

Very different from the ssp spectra, all the ppp spectra show the same spectral features with no film thickness dependence. And the two strong modes at 2912 cm^{-1} and 2960 cm^{-1} in the surface ppp spectra (Figure 2) did not appear here. Remarkably, the ppp spectral features for the PBMA films on the Ag substrates, which are the ss mode at 2875 cm^{-1} and Fermi resonance at 2935 cm^{-1}, as shown in Panel C of Figure 5, are similar to those for the sandwiched geometry. This suggests that the observed ppp vibrational resonances for the PBMA films on the Ag substrates were not from the surface in air but from the PBMA/Ag interface.

Considering the non-resonant background (~260 in Panel C of Figure 5) generated from the Ag surface using ppp polarization combination, such a strong non-resonant background was closely related to the surface plasmon polariton (SPP) pumped by the p-polarized visible light [32]. Being localized at the PBMA/Ag interface, the Ag SPP can couple with the molecular vibrations of PBMA at the PBMA/Ag interface but cannot affect the molecular vibrations of PBMA at the surface due to its fast evanescence along the surface normal. This is the intrinsic reason why the PBMA/Ag interfacial resonant signals can be observable while the PBMA surface resonant signals in air were not observed for ppp polarization combination. This should also be the reason why ppp spectra for this geometry and the sandwiched geometry are similar since both resonant signals came from the molecular vibrations at the PBMA/Ag interface. Such a contribution from SPP due to the optical nature of the metals is very important on detecting the molecular structures at the buried polymer/metal interfaces. Here we won't go into details since it is beyond the scope of this study. However we still give the calculated Fresnel coefficients of the ppp polarization combination for the PBMA surface in air and the PBMA/Ag interface as a comparison to the sandwiched geometry, as shown in

Panels B and C of Figure 6.

3.4 Comparison of the different experimental geometries and the spectral characteristics

The three different experimental geometries have been discussed, i.e. a PBMA thin film on the silica substrate, PBMA thin films sandwiched between silica and Ag, and PBMA thin films directly deposited on the Ag substrates. As we discussed in the C-H infrared frequency range (2800 cm^{-1}~3050 cm^{-1}), for a PBMA thin film on the silica substrate, the surface signals dominate the SFG spectra, whether for ssp or ppp polarization combinations. For a PBMA thin film sandwiched between silica and Ag, the PBMA/Ag interfacial signals dominate the spectra for both ssp and ppp polarization combinations. For a PBMA thin film deposited on the Ag substrate, the surface signals dominate the spectrum for the ssp polarization combination while the PBMA/Ag interfacial signals dominate the spectrum for the ppp polarization combination. Polar orders of the side butyl methyl groups were found at both the surface in air and the PBMA/Ag interface. For the PBMA surface spectra, as shown in Figure 2, the ss mode (2880 cm^{-1}) and Fermi resonance (2935 cm^{-1}) of the ester butyl methyl groups dominate the ssp spectrum while the as mode (2960 cm^{-1}) of the ester butyl methyl groups dominates the ppp spectrum. For the spectra of the PBMA/Ag interface, as shown in Figure 3, the as mode (2956 cm^{-1}) dominates the ssp spectra while the ss mode (2875 cm^{-1}) and Fermi resonance (2935 cm^{-1}) dominate the ppp spectrum. Such distinct spectral difference strongly suggests the ester butyl methyl groups at the surface and the buried PBMA/Ag interface have very difference orientational orderings. For a more accurate description, using the fitted results for the spectra of the PBMA thin film on the silica (Figure 2) and the sandwiched geometry (Figure 3), we deduced the possible tilt angles of ester butyl methyl groups at the PBMA surface in air and the buried PBMA/Ag interface. For the PBMA surface in air, the ratio of the ssp and ppp effective nonlinear susceptibility components $\chi^{(2)}_{eff,ssp,ss}\big/\chi^{(2)}_{eff,ppp,as}$ was used. For the PBMA/Ag interface, the ratio of the ssp and ppp effective nonlinear susceptibility components $\chi^{(2)}_{eff,ssp,as}\big/\chi^{(2)}_{eff,ppp,ss}$ was used. Such ratios can be related to the tilt angle θ of the ester butyl methyl groups via the following equations [33-36].

$$\left|\frac{\chi^{(2)}_{eff,ssp,ss}}{\chi^{(2)}_{eff,ppp,as}}\right| \cong \left|\frac{0.40\langle\cos\theta\rangle + 0.20\langle\cos^3\theta\rangle}{1.5(\langle\cos\theta\rangle - \langle\cos^3\theta\rangle)}\right| \quad (6\text{-}1)$$

$$\left|\frac{\chi^{(2)}_{eff,ssp,as}}{\chi^{(2)}_{eff,ppp,ss}}\right| \cong \left|\frac{0.90(\langle\cos\theta\rangle - \langle\cos^3\theta\rangle)}{3.1\langle\cos\theta\rangle - 0.79\langle\cos^3\theta\rangle}\right| \quad (6\text{-}2)$$

The details related to the tilt angle calculation can be found in Supplementary Information. Figure 7 shows the calculated curves of $\left|\chi^{(2)}_{eff,ssp,ss}/\chi^{(2)}_{eff,ppp,as}\right|$ for the PBMA surface in air (Panel A) and $\left|\chi^{(2)}_{eff,ssp,as}/\chi^{(2)}_{eff,ppp,ss}\right|$ for the PBMA/Ag interface (Panel B) in terms of the tilt angle. Such ratios as a function of the averaged tilt angle (θ_0) with different root-mean-square distribution width (σ) were also plotted. From the intersection points between the plotted curves and the experimental values (Panel A: 2.4 for the PBMA surface in air; Panel B: 0.28 for the PBMA/Ag interface), the possible tilt angles of the side ester butyl methyl groups can be deduced: at the PBMA surface in air, the ester butyl methyl groups adopt a small tilt angle or like to "stand up"; at the PBMA/Ag interface, the ester butyl methyl groups adopt a large tilt angle or like to "lie down".

4. Conclusions

As a surface and interfacial sensitive analytical tool, SFG vibrational spectroscopy has been applied to study the polymer surfaces and interfaces for more than one decade. In this paper, a unified description using three SFG experimental geometries was given to illustrate the molecular structures of the buried PBMA/Ag interface with comparison to the PBMA surface in air. According to the experimental results, the ester butyl methyl groups at the buried PBMA/Ag interface are polar-ordered as well as those at the PBMA surface in air. However, the ester butyl methyl groups at the buried PBMA/Ag interface adopt a large tilt angle while the ester butyl methyl groups at the PBMA surface in air adopt a small tilt angle. Such SFG results reflect the inherently different nature of the buried interface from that of the surface, i.e. same molecular groups at the surface and the buried interface could have very different orientational orderings. We believe this study will provide a useful experimental and analytical framework and intrigue more studies on elaborating the molecular structures of the buried polymer/metal interfaces by using SFG vibrational spectroscopy.

Acknowledgments:

References:

1. M. Fleischmann, P. J. Hendra, A. J. McWuillan *Chem. Phys. Lett.* **1974**, *26*, 163-166.

2. R. P. Van Duyne *Chem. Biochem. Appl. Lasers* **1979**, *4*, 101-185.

3. H. Ade, H. Stoll *Nat. Mater.* **2009**, *8*, 281-290.

4. G. Hahner *Chem. Sov. Rev.* **2006**, *35*, 1244-1255.

5. Y. R. Shen *Nature* **1989**, *337*, 519-525.

6. K. B. Eisenthal *Chem. Rev.* **1996**, *96*, 1343-1360.

7. M. Buck, M. Himmelhaus *J. Vac. Sci. Technol. A* **2001**, *19*, 2717-2736

8. Z. Chen, Y. R. Shen, G. A. Somorjai *Annu. Rev. Phys. Chem.* **2002**, *53*, 437-465.

9. G. L. Richmond *Chem. Rev.* **2002**, *102*, 2693-2724.

10. F. M. Geiger *Annu. Rev. Phys. Chem.* **2009**, *60*, 61-83.

11. Z. Chen *Prog. Polym. Sci.* **2010**, 35, 1376-1402.

12. K. S. Gautam, A. D. Schwab, A. Dhinojwala, D. Zhang, S. M. Dougal, M. S. Yeganeh
    Phys. Rev. Lett. **2000**, 85, 3854–3857.

13. K. S. Gautam, A. Dhinojwala *Phys. Rev. Lett.* **2002**, 88, 145501.

14. H. Tsuruta, Y. Fujii, N. Kai, H. Kataoka, T. Ishizone, M. Doi, H. Morita, K. Tanaka
    Macromolecules **2012**, 45, 4643-4649.

15. X. Lu, N. Shephard, J. Han, G. Xue, Z. Chen *Macromolecules* **2008**, 41, 8770-8777.

16. X. Lu, D. Li, C. B. Kristalyn, J. Han, N. Shephard, S. Rhodes, G. Xue, Z. Chen
    Macromolecules **2009**, 42, 9052-9057.

17. X. Lu, G. Xue, X. Wang, J. Han, X. Han, J. Hankett, D. Li, Z. Chen *Macromolecules*
    2012, 45, 6087-6094.

18. Y. R. Shen *The Principles of Nonlinear Optics*; Wiley: New York, 1984.

19. X. Zhuang, P. B. Miranda, D. Kim, Y. R. Shen Phys. Rev. B 1999, 59, 12632-12640.

20. Y. R. Shen *Annu. Rev. Phys. Chem.* **1989**, 40, 327-350.

21. M. B. Feller, W. Chen, Y. R. Shen *Phys. Rev. A* **1991**, 43, 6778-6792.

22. P. Guyot-Sionnest, J. H. Hunt, Y. R. Shen *Phys. Rev. Lett.* **1987**, 59, 1597-1600.

23. X. Wei, S. C. Hong, A. I. Lvovsky, H. Held, Y. R. Shen *J. Phys. Chem. B* **2000**, 104, 3349-3354.

24. J. Wang, C. Chen, S. M. Buck, Z. Chen *J. Phys. Chem. B* **2001**, 105, 12118-12125.

25. X. Lu, M. L. Clarke, D. Li, X. Wang, G. Xue, Z. Chen *J. Phys. Chem. C* **2011**, 115, 13759-13767.

26. J. Wang, Z. Paszti, M. A. Even, Z. Chen *J. Am. Chem. Soc.* **2002**, 124, 7016-7023.

27. M. B. Feller, W. Chen, Y. R. Shen *Phys. Rev. A* **1991**, 43, 6778-6792.

28. D. Wilk, D. Johannsmann, C. Stanners, Y. R. Shen *Phys. Rev. B* **199**5, 51, 10057-10067.

29. S. J. McGall, P. B. Davies, D. J. Neivandt *J. Phys. Chem. B* **2004**, 108, 16030-16039.

30. Y. Tong, Y. Zhao, N. Li, M. Osawa, P. B. Davies, S. Ye *J. Chem. Phys.* **2010**, 133, 034704.

31. E. H. G. Backus, N. Garcia-Araez, M. Bonn, H. J. Bakker *J. Phys. Chem. C* **2012**, 116, 23351-23361.

32. A. Liebsch *Appl. Phys. B* **1999**, 68, 301-304.

33. C. Hirose, N. Akamatsu, K. Domen *Appl. Spectrosc.* **1992**, 46, 1051–1072.

34. C. Hirose, N. Akamatsu, K. Domen *J. Chem. Phys.* **1992**, 96, 997-1004.

35. X. Wei, X. Zhuang, S. C. Hong, T. Goto, Y. R. Shen *Phys. Rev. Lett.* **1999**, 82, 4256-4259.

36. G. J. Simpson, L. K. Rowlen *J. Am. Chem. Soc.* **1999**, 121, 2635-2636.
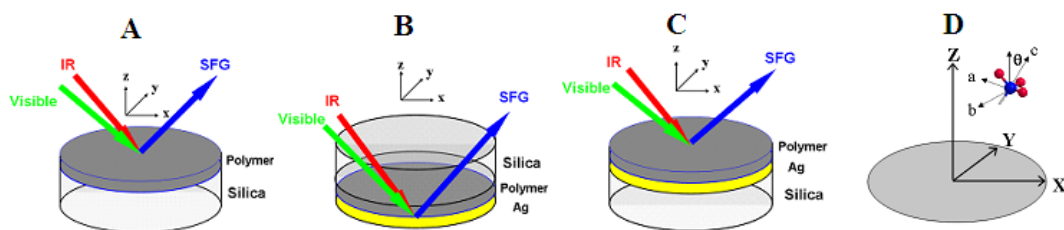
Figures and figure captions

Figure 1. The three difference sample geometries for the SFG measurement and the defined tilt angle. A: a polymer film on a silica substrate; B: a polymer thin film sandwiched between a silica window and a Ag substrate; C: a polymer thin film on a Ag substrate which was previously prepared on a silica window; D: the lab fixed coordinate system is defined as (x, y, z) system and the molecular coordinate system of a methyl group is defined as the (a, b, c) system, z axis defined as the surface normal and xz plane containing the input and ouput beams, c is the principal axis of the methyl group, ac plane contains one C-H bond and b is perpendicular to ac plane. Tilt angle is defined as the angle between z axis and c axis.
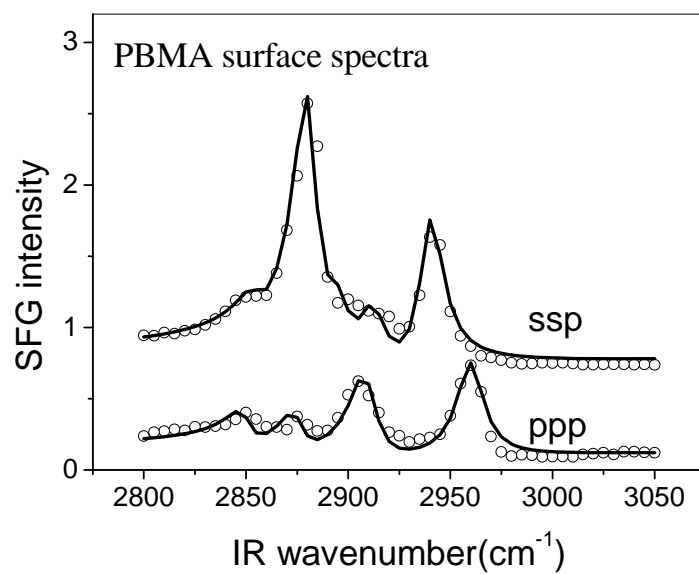
Figure 2. SFG spectra of the PBMA surface collected from a PBMA film on a silica window (Panel A in Figure 1). Solid lines are the fitted curves.
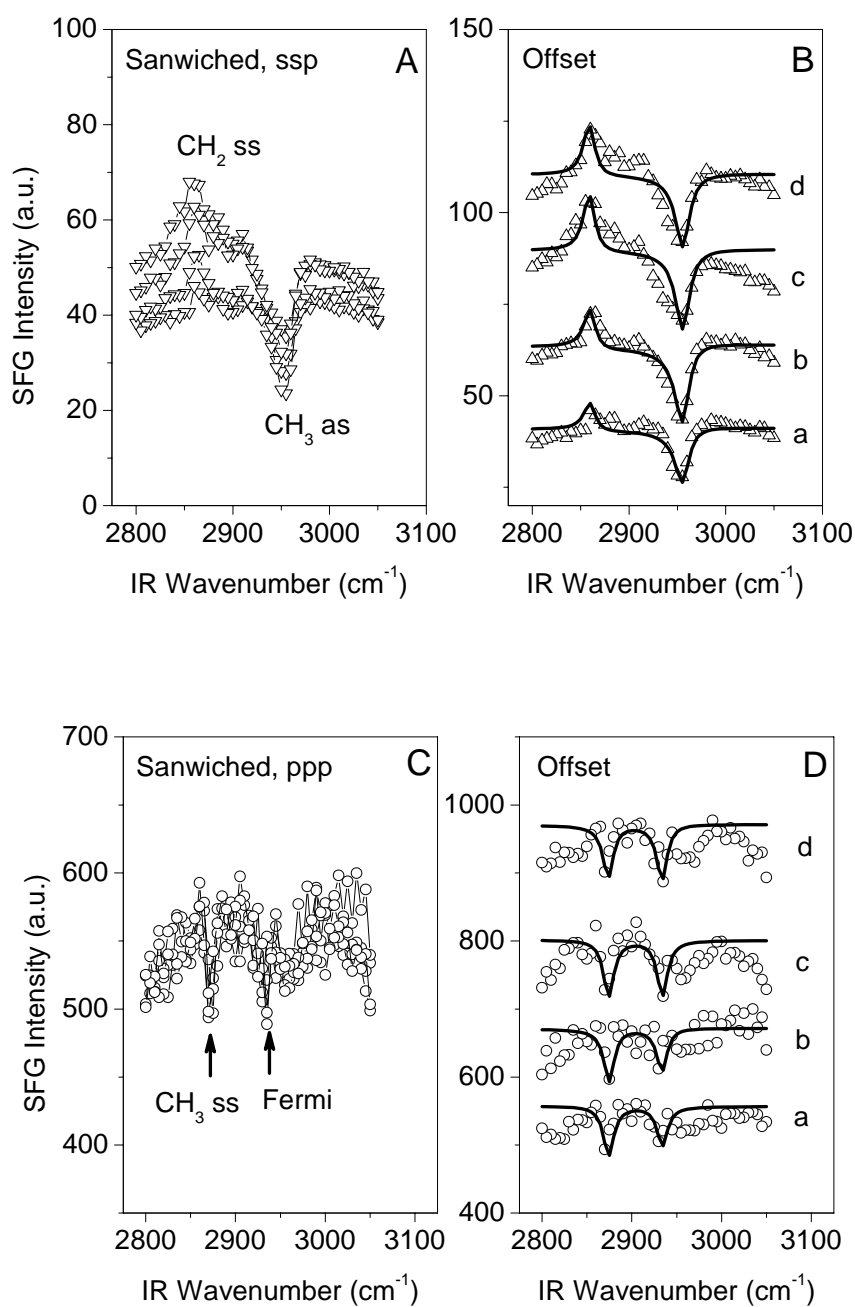
Figure 3. Collected ssp and ppp spectra for the PBMA films sandwiched between the silica windws and Ag substrates; the PBMA film thicknesses of sample a, b, c, and d were 24, 56, 85, and 113 nm, respectively. Original spectra were in Panel A and Panel C; the spectra in Panel B and Panel D were offset for clarity. Solid lines were the fitted curves.
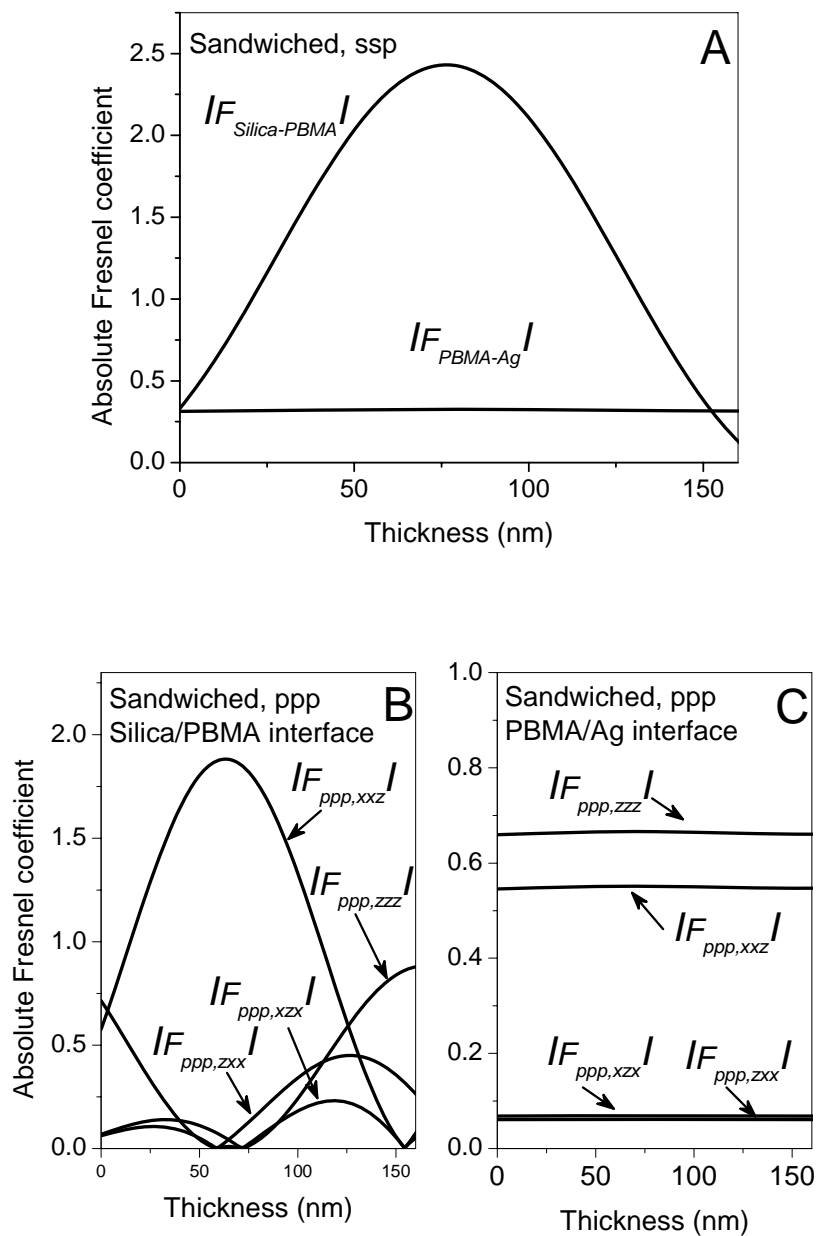
Figure 4. The calculated absolute Fresnel coefficients for the sanwiched geometry. Panel A: ssp polarization combiantion; Panel B: ppp polarization combination for the silica/PBMA interface; Panel C: ppp polarization combination for the PBMA/Ag interface.
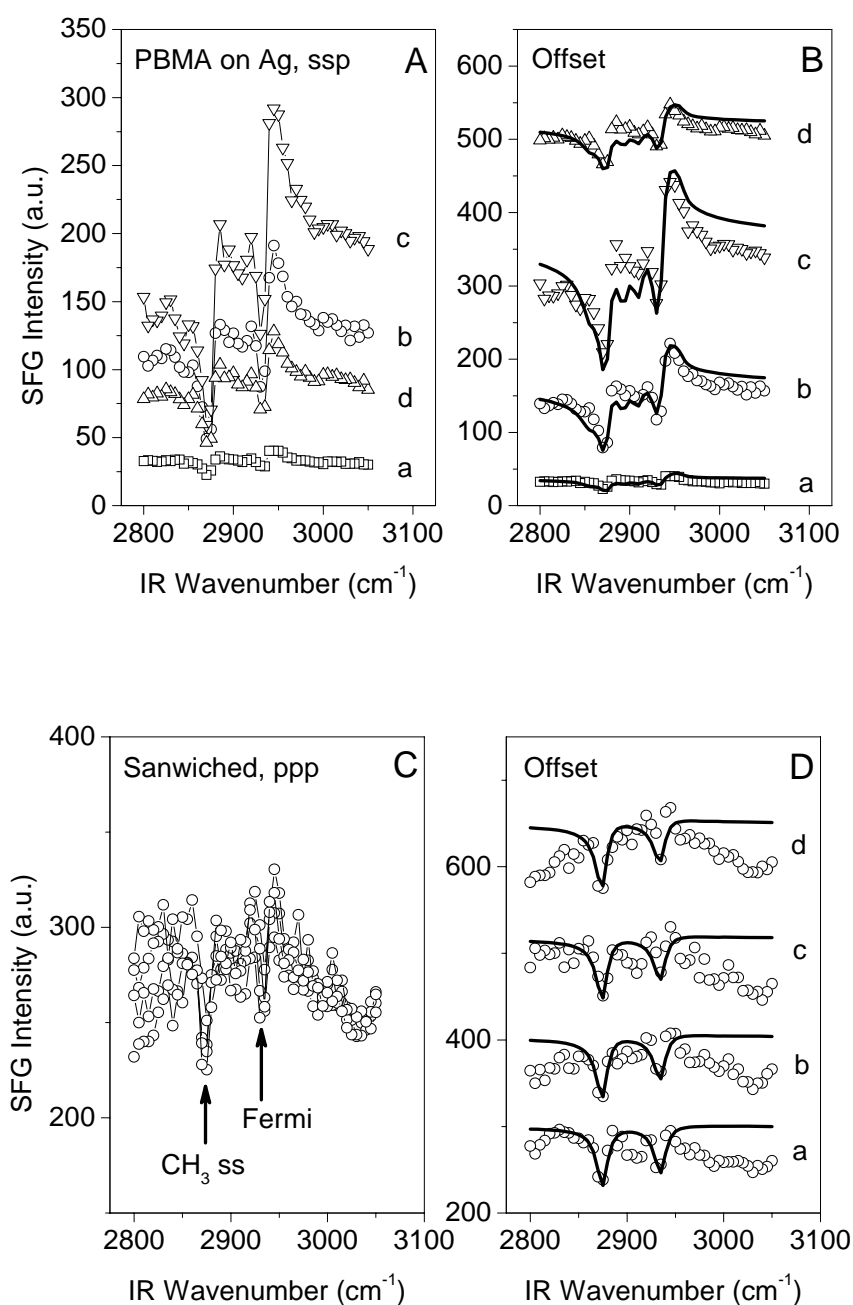
Figure 5. Collected ssp and ppp spectra for the PBMA films on the Ag substrates; the PBMA film thicknesses of sample a, b, c, and d were 11, 33, 45, and 127 nm, respectively. Original spectra were in Panel A and Panel C; the spectra in Panel B and Panel D were offset for clarity. In Panel B, the ssp spectra reconstructed from the PBMA surface in air and the PBMA/Ag interface were also shown.
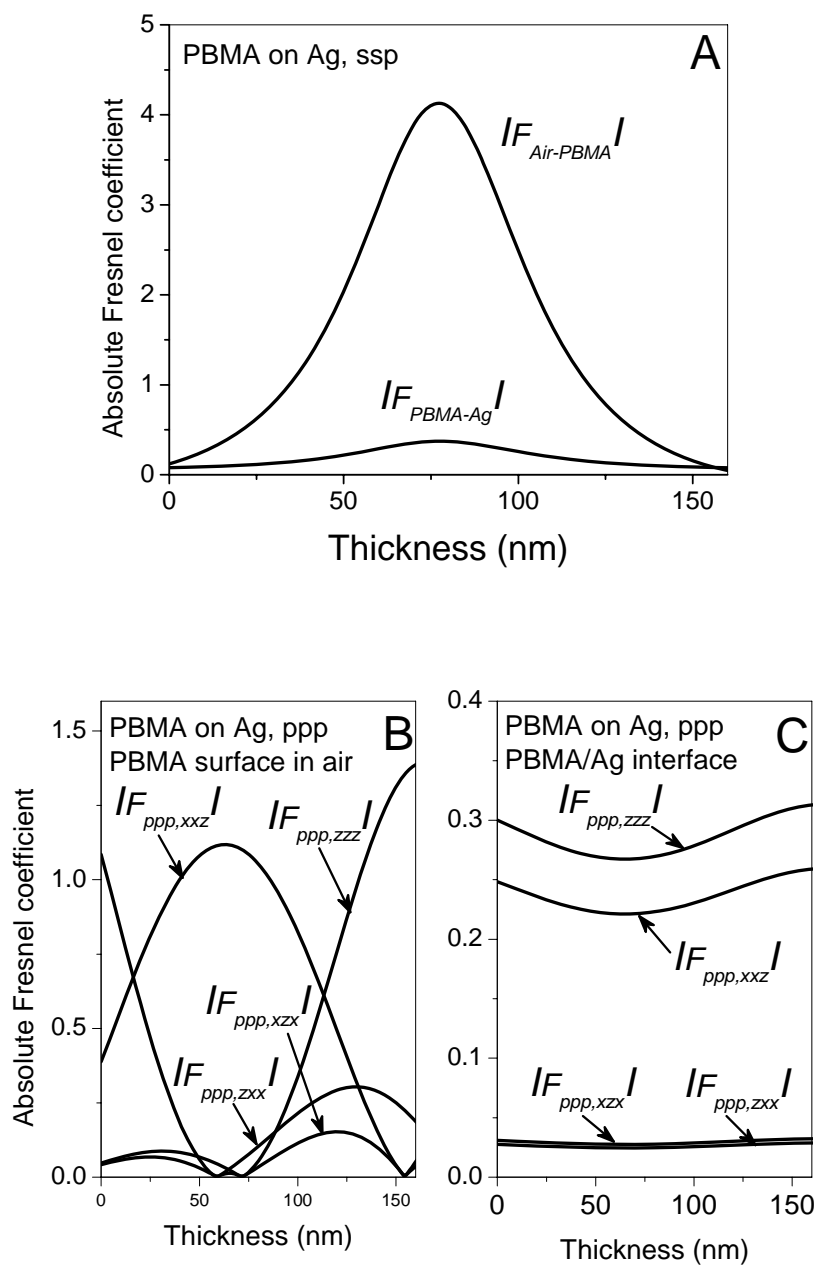
Figure 6. The calculated absolute Fresnel coefficients for the sandwiched geometry. Panel A: ssp polarization combination; Panel B: ppp polarization combination for the silica/PBMA interface; Panel C: ppp polarization combination for the PBMA/Ag interface.

21
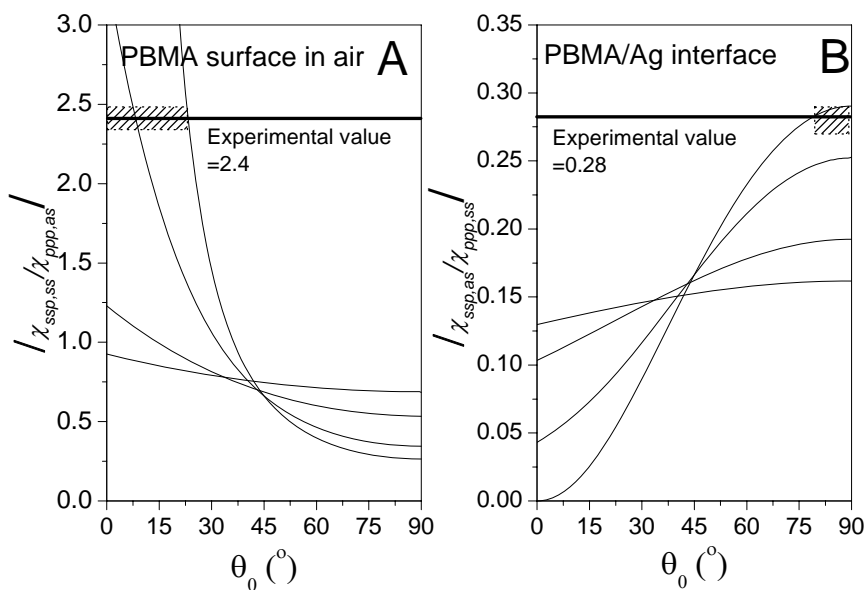
Figure 7. Theoretical curves of $\left|\chi^{(2)}_{eff,ssp,ss}\big/\chi^{(2)}_{eff,ppp,as}\right|$ for the PBMA surface in air (Panel A) and

$\chi^{(2)}_{eff,ssp,as}\big/\chi^{(2)}_{eff,ppp,ss}$ for the PBMA/Ag interface (Panel B) as a function of tilt angle θ_0 and angle

distribution σ; the intersection points suggest the possible ester butyl methyl tilt angles with angle distribution. In Panel B, the experimental value of 0.28 was from the SFG spectra of a sandwich PBMA thin film with a thickness of 85 nm.

22

Table 1. Fitting results for the SFG spectra of the PBMA surface in Figure 1.

Wavenumber (cm^{-1})	ssp		ppp		Assignment
	A_q	Γ_q	A_q	Γ_q	
2857	1.0	7	1.9	7	CH$_2$ (ss)
2880	7.5	7	2.3	7	(ester butyl) CH$_3$ (ss)
2895	3.2	8	-	-	unassigned
2912	3.5	8	5.5	8	- CH$_2$ (as)
2935	6.4	7	-	-	Fermi
2960	-	-	6.7	8	CH$_3$ (as)

Table 2. Fitting results for the SFG spectra of the sandwiched geometry in Figure 3. A for ssp polarization combination and B for ppp polarization combination.

A (ssp)						
Thickness (nm)	2860 cm^{-1} (CH$_2$ ss)		2956 cm^{-1} (ester butyl CH$_3$ as)		χ_{NR}	Phase (rad)
	A_q	Γ_q	A_q	Γ_q		
24	4.3	7	-10.1	9	6.4	1.8
56	7.0	7	-12.4	9	6.4	1.7
85	6.7	7	-11.5	9	7.3	1.7
113	6.9	7	-11.3	9	6.9	1.7

B (ppp)						
Thickness (nm)	2875 cm^{-1} (ester butyl methyl CH$_3$ ss)		2935 cm^{-1} (Fermi)		χ_{NR}	Phase (rad)
	A_q	Γ_q	A_q	Γ_q		
24	14.2	7	14.0	7	23.6	-1.6
56	14.8	7	13.5	7	24.1	-1.6
85	16.7	7	15.5	7	24.5	-1.7
113	15.5	7	15.3	7	24.3	-1.6

Table 3. Fitting results for the ppp spectra in Panle C of Figure 5.

Thickness (nm)	2875 cm^{-1} (ester butyl methyl CH$_3$ ss)		2935 cm^{-1} (Fermi)		χ_{NR}	Phase (rad)
	A_q	Γ_q	A_q	Γ_q		
11	14.3	7	11.5	7	17.3	-1.4
33	14.8	7	10.8	7	17.4	-1.3
45	14.4	7	10.3	7	17.8	-1.3
127	16.1	7	10.2	7	17.3	-1.2